THE JOURNAL OF BIOLOGICAL CHEMISTRY VOL. 286, NO. 23, pp. 20892–20900, June 10, 2011

Structural Basis of Neutralization of the Major Toxic Component from the Scorpion *Centruroides noxius* Hoffmann by a Human-derived Single-chain Antibody Fragment*[S]

Received for publication, March 8, 2011, and in revised form, March 30, 2011 Published, JBC Papers in Press, April 13, 2011, DOI 10.1074/jbc.M111.238410

Juan Carlos Canul-Tec[‡1], Lidia Riaño-Umbarila[‡], Enrique Rudiño-Piñera[‡], Baltazar Becerril[‡], Lourival D. Possani[‡2], and Alfredo Torres-Larios[§3]

From the [‡]Departamento de Medicina Molecular y Bioprocesos, Instituto de Biotecnología, Universidad Nacional Autónoma de México, Apartado Postal 510-3, Cuernavaca, Morelos 62210 and the [§]Departamento de Bioquímica y Biología Estructural, Instituto de Fisiología Celular, Universidad Nacional Autónoma de México, Circuito Exterior s/n, Ciudad Universitaria, Apartado postal 70-243, Mexico City 04510, México

It has previously been reported that several single-chain antibody fragments of human origin (scFv) neutralize the effects of two different scorpion venoms through interactions with the primary toxins of *Centruroides noxius* Hoffmann (Cn2) and *Centruroides suffusus suffusus* (Css2). Here we present the crystal structure of the complex formed between one scFv (9004G) and the Cn2 toxin, determined in two crystal forms at 2.5 and 1.9 Å resolution. A 15-residue span of the toxin is recognized by the antibody through a cleft formed by residues from five of the complementarity-determining regions of the scFv. Analysis of the interface of the complex reveals three features. First, the epitope of toxin Cn2 overlaps with essential residues for the binding of β-toxins to its Na^+ channel receptor site. Second, the putative recognition of Css2 involves mainly residues that are present in both Cn2 and Css2 toxins. Finally, the effect on the increase of affinity of previously reported key residues during the maturation process of different scFvs can be inferred from the structure. Taken together, these results provide the structural basis that explain the mechanism of the 9004G neutralizing activity and give insight into the process of directed evolution that gave rise to this family of neutralizing scFvs.

The most harmful components of scorpion venoms are toxins that can selectively bind to voltage-gated ion channels and affect their modulation. A subgroup among these toxins, the long chain Na^+ channel toxins, are formed by 60–70-amino acid peptides, which adopt a highly packed core with a βαββ-fold (1). These Na^+ channel toxins have further been classified into two major classes (α and β) based on their effects in the gating mechanism of Na^+ channels and their properties (2–4). The old world toxin II from *Androctonus Australia* Hector (AaHII) and the new world toxin II from *Centruroides suffusus suffusus* (Css2)[4] are considered to be the archetypes of α- and β-toxins active against mammals, respectively (3, 5).

The buthid scorpion, *C. suffusus suffusus*, is one of the most poisonous to the rural human population in the Northwest of Mexico. The most noxious and abundant molecule found in the venom of this scorpion is Css2 (LD_{50} of 0.7 μg/20 g of mice of the strain CD1) (6). In addition, the Mexican scorpion *Centruroides noxius* Hoffmann produces toxin Cn2, one of the most abundant and noxious peptides against mammals (LD_{50} of 0.25 μg/20 g of mice of the strain CD1) (7). Sequence comparison shows that Cn2 presents a high similarity with other β-toxins from *C. suffusus suffusus,* such as Css2 and Css4 (around 90%, see below). Both toxins, Cn2 and Css2, are specific to Na^+ channel subtype Na_v 1.6 (6, 8).

Due to the fact that scorpion stings are a considerable public health issue in a number of countries (9), efforts have been put forth to explore alternative technologies to generate more specific antibodies against the venom of scorpions harmful to humans (reviewed in Ref. 10). One of the most promising alternatives to classical antivenoms is the use of antibodies of human origin. Riaño-Umbarila *et al.* (11) constructed a non-immune human antibody library. A single-chain antibody fragment (scFv), designated 3F, which recognizes the toxin Cn2, was isolated by phage display technology. After three cycles of directed evolution, the authors selected scFv 6009F, which binds with picomolar affinity to Cn2. From 3F, but following a different evolutionary route against toxin Css2, the antibody variant scFv 9004G was found (12). Notably, both antibodies neutralize the whole venom of *C. noxius* and *C. suffusus suffusus* (12). Combinations of key residue changes from both antibodies resulted in scFv LR, an antibody fragment with a higher level of expression and better stability.

* This work was supported by Grant P-156 from Instituto Bioclon (to L. D. P.), Consejo Nacional de Ciencia y Tecnología Grant 60127-Q (to A. T.-L.), Programa de Apoyo a Proyectos de Investigación e Innovación Tecnológica, Universidad Nacional Autónoma de México (PAPIIT) Grants IN202910 (to A. T.-L.) and IN204110 (to L. D. P.), and Instituto de Ciencia y Tecnología del Distrito Federal Grant PIFUTP09-279 (to A. T.-L.).

The atomic coordinates and structure factors (codes 2YBR and 2YC1) have been deposited in the Protein Data Bank, Research Collaboratory for Structural Bioinformatics, Rutgers University, New Brunswick, NJ (http://www.rcsb.org/).

[S] The on-line version of this article (available at http://www.jbc.org) contains supplemental Tables S1–S3 and Figs. S1–S8.

[1] Recipient of Consejo Nacional de Ciencia y Tecnología Scholarship 45248.

[2] To whom correspondence may be addressed: Av. Universidad 2001, Colonia Chamilpa, Cuernavaca 62210, México. Tel.: 52-777-3171209; E-mail: possani@ibt.unam.mx.

[3] To whom correspondence may be addressed. Fax: 52-55-5622-5630; E-mail: torres@ifc.unam.mx.

[4] The abbreviations used are: Css2, *C. suffusus suffusus* toxin II; Cn2, *C. noxius* Hoffmann toxin; ScFV, single-chain antibody fragment; CDR, complementarity-determining region; Bis-Tris, 2-(bis(2-hydroxyethyl)amino)-2-(hydroxymethyl)propane-1,3-diol.

Despite previous biochemical and immunological studies, the localization of the toxin epitope and a structural perspective on the structure-function relationship of the different scFvs remained elusive. Here we present the crystal structures of the 9004G-Cn2 complex in two crystal forms at 2.5 and 1.9 Å resolution. The structure analysis shows that a common binding region of the toxin, comprising the segments that run from the β_1 strand to the α-helix (Tyr^{14}–Leu^{19}) and the β-turn (Tyr^{42}–Ala^{45}) that connects the β_2 and β_3 strands, is shared by the antibody 9004G and the Na^+ channels. These observations imply that 9004G neutralizes Cn2 by competing for a set of residues that form the bioactive surface of Cn2 and therefore blocks the receptor binding site.

EXPERIMENTAL PROCEDURES

Cn2 Toxin Purification—Cn2 toxin was extracted from the soluble venom of the scorpion *C. noxius* Hoffmann and was purified by a series of chromatographic steps that included size exclusion chromatography followed by several rounds of cation exchange chromatography, as described previously (7). Fractions containing Cn2 were pooled, lyophilized, and further purified by high performance liquid chromatography (HPLC). For the HPLC purification, Cn2 aliquots were loaded onto an analytical C18 reverse-phase column (Vydac, Hesperia, CA) in the presence of solvent A (0.1% TFA in water) and eluted with a linear gradient from 20 to 40% of solvent B (0.1% of trifluoroacetic acid in acetonitrile) over 20 min at a flow rate of 1 ml/min. The homogeneity of Cn2 was verified by mass spectrometry analysis using a Finnigan LCQ^{DUO} ion trap mass spectrometer (Thermo Finnigan). Fractions containing the Cn2 toxin were pooled, vacuum-dried, and stored at −20 °C until needed.

Antibody scFv 9004G Expression and Purification—Recombinant antibody scFv 9004G was expressed with a C-terminal c-Myc tag followed by a His_6 affinity purification tag in *Escherichia coli* TG1 cells, as described previously (11). Cells were grown at 37 °C until an A_{600} of 0.9 was reached. At that time, cells were induced for 6 h with a final concentration of 1 mM isopropyl-β-D-thiogalactopyranoside at 30 °C and were harvested by centrifugation (5,515 × *g* for 10 min). The resulting cell pellet from 2 liters of culture was frozen at −80 °C until needed. For scFv 9004G purification, the cell pellet was thawed and resuspended in 20 ml of buffer A (20 mM sodium phosphate, pH 7.4, 500 mM sodium chloride, 40 mM imidazole). Cells were lysed by sonication on ice and then centrifuged at 20,410 × *g* for 30 min. The resulting supernatant was applied onto a 5-ml Ni^{2+}-Sepharose FF column (GE Healthcare) connected to an Äkta FPLC system (GE Healthcare). The column was then washed with buffer A to elute nonspecifically bound proteins. The antibody was eluted with buffer A plus 160 mM imidazole. The fraction containing scFv 9004G was applied to two desalting columns (HiPrep 26/10, GE Healthcare) connected in tandem and previously equilibrated with 40 mM Tris, pH 8.5. Fractions containing the scFv 9004G were pooled and then applied to a MonoQ 10/100 column pre-equilibrated with 40 mM Tris, pH 8.5. The antibody was eluted with a linear gradient of NaCl from 0 to 200 mM in 40 mM Tris, pH 8.5. Fractions containing the antibody were pooled, diluted with 3 volumes of 40 mM Tris, pH 8.5, and applied to an ANX Sepharose FF column (GE Healthcare), previously pre-equilibrated with buffer B. The protein was again eluted with a linear gradient of NaCl from 0 to 200 mM in 40 mM Tris, pH 8.5. Finally, fractions containing the scFv 9004G were pooled and concentrated (Amicon Ultra filter, Millipore, 30 kDa) to 1 mg/ml. The protein sample was >99% pure as judged by denaturing gel electrophoresis.

Formation of the 9004G-Cn2 Complex—Protein aliquots of scFv 9004G and toxin Cn2 were dialyzed in PBS (137 mM NaCl, 2.7 mM KCl, 8 mM Na_2HPO_4, 1.5 mM KH_2PO_4, pH 7.2). Complex 9004G-Cn2 was formed by mixing Cn2 with scFv 9004G (1.3:1 ratio) and incubating the reaction for 1 h at room temperature with mild agitation. The complex was then concentrated to ~7 mg/ml (Amicon Ultra filter, Millipore, 30 kDa). The 9004G-Cn2 complex was loaded onto a size exclusion chromatography Superdex S-75 10/300 analytical column (GE Healthcare) connected to an Äkta FPLC system (GE Healthcare) equilibrated with PBS. The column was run at a flow rate of 1 ml/min, and absorbance was monitored at 280 nm. Two peaks were eluted, corresponding to the dimeric and monomeric forms of the complex 9004G-Cn2. The major, monomeric peak of the complex 9004G-Cn2 was collected and concentrated to ~20 mg/ml.

Crystallization of the 9004G-Cn2 Complex and Data Collection—Crystals of the 9004G-Cn2 complex were obtained both by vapor diffusion using a sitting-drop setup and also by microbatch crystallization methods, at 19 °C. Via vapor diffusion, crystals appeared within 1 week in a drop containing 1 μl of a solution of the 9004G-Cn2 complex at 5 mg/ml and 1 μl of reservoir solution consisting of 100 mM Bis-Tris, pH 5.5, 25% polyethylene glycol 3350, and 200 mM ammonium sulfate. Crystals were cryoprotected by increasing the concentration of polyethylene glycol 3350 in the crystal drop to 35%. Crystals obtained with the microbatch method appeared after 2 weeks in a drop containing 1 μl of a solution of the 9004G-Cn2 complex at 7.9 mg/ml and 1 μl of 1.4 M Na_2HPO_4/K_2HPO_4, pH 5.6, under paraffin oil. These crystals were cryoprotected, replacing the water in the mother liquor by 25% glycerol (v/v). Crystals were then flash-frozen in liquid nitrogen. Diffraction data were collected at the Life Sciences Collaborative Access Team (LS-CAT) 21-ID-F and G beamlines at the Advanced Photon Source (Argonne National Laboratory). Data were indexed with MOSFLM (13) and XDS (14) and reduced with SCALA (15).

Structure Determination and Refinement—The structure of the 9004G-Cn2 complex was determined by molecular replacement using PHASER (16) in the $P2_12_12_1$ (data collected at 2.5 Å resolution) and F23 space groups (data collected at 1.9 Å resolution). The search models that gave rise to the initial phases were generated by dividing a model of the 6009F-Cn2 complex[5] into three parts (the heavy and light variable domains of 6009F and toxin Cn2) and submitting these three partial models as separate search ensembles (Z-scores for the rotation and translation functions, respectively: 7.0 and 10.9, 6.0 and 20.4, and 6.1 and 25.9 for the three molecules in the asymmetric unit of the light (L) chain; 7.1 and 33.6, 6.1 and 28.1, and 5.7 and 26.5 for the heavy (H) chain; 5.4 and 22.3, 4.4 and 18.9, and 4.4 and 33.3

[5] M. Domínguez-Laguna, Lidia Riaño-Umbarila, and Baltazar Becerril, unpublished data.

TABLE 1
X-ray data collection and refinement statistics
Values in parentheses are for the last resolution shell.

Parameters	Values	
Data collection statistics		
Space group	$P2_12_12_1$	F23
Unit cell dimensions		
a, *b*, *c* (Å)	69.8, 104.5, 152.5	219.7, 219.7, 219.7
α, β, γ angles (degrees)	90.0, 90.0, 90.0	90.0, 90.0, 90.0
Resolution range (Å)	46.20–2.55 (2.69–2.55)	54.94–1.90 (2.00–1.90)
No. of reflections	238,909 (34,895)	789,205 (113,816)
No. of unique reflections	37,179 (5,378)	68,864 (9,978)
Data completeness (%)	99.9 (100.0)	100.0 (100.0)
R_{sym} (%)	9.5 (33.4)	7.5 (29.6)
I/σ	6.4 (2.3)	6.3 (2.5)
$Mn(I)/\sigma$	14.2 (5.1)	22.2 (8.1)
No. of complexes in asymmetric unit	3	2
Refinement statistics		
Resolution range (Å)	45.72–2.55 (2.62–2.55)	42.28–1.90 (1.95–1.90)
R_{cryst}/R_{free} (%)	19.1 (30.5)/24.6(32.5)	18.6 (23.1)/21.2 (26.6)
No. of atoms, protein/ligands/solvent	6,721/NA[a]/220	4,532/54/568
Mean B value, protein/ligands/solvent (Å^2)	32.9/NA/29.0	23.4/38.6/33.3
B value from Wilson plot (Å^2)	32.8	20.1
Root mean square deviation bond lengths (Å)	0.01	0.01
Root mean square deviation bond angles (degrees)	1.26	1.12
Cross-validated σA coordinate error	0.48	0.12
Residues in Ramachandran plot (%)		
Most allowed region	645 (89.3%)	439 (91.1%)
Allowed region	74 (10.2%)	39 (8.1%)
Generously allowed region	3 (0.4%)	2 (0.4%)
Disallowed region[b]	0 (0.0%)	2 (0.4%)

[a] NA, not applicable.
[b] No σ cut-offs used on the refinement ($F > 0\sigma F$).

for the Cn2 toxin). Tight non-crystallographic symmetry restraints were imposed at the beginning of the refinement of the structure at 2.5 Å resolution among the three copies of the complex in the asymmetric unit. The restraints were released during the last cycles of refinement. Since initial refinement, difference maps showed the 10 changes that exist between 9004G and 6009F scFvs (see Fig. 1). The structure of the 9004G-Cn2 complex in space group F23, with two complexes in the asymmetric unit, was solved using the coordinates of the first 9004G-Cn2 complex as the search model (Z-scores: 9.3 and 29.9 for the rotation and translation functions, respectively, for one complex and 10.8 and 55 for the second complex in the asymmetric unit). Refinement was performed using REFMAC (15) and Phenix (17). Refinement was alternated with manual building/refinement in COOT (18). Five percent of the data were used to validate the refinement. Water molecules were first located using the program ARP/wARP (19) and then validated in COOT. Refinement concluded in REFMAC after the addition of alternate side-chain conformations. σA-weighted $F_o - F_c$ simulated annealing omit maps were used to further validate the quality of the model and the presence of water molecules. Data collection and refinement statistics are summarized in Table 1.

Structure Analysis—Quality of the final model was evaluated using PROCHECK (20) and the RCSB validation server ADIT!. Superposition and location of invariant water molecules were made using the program 3dss (21). Interfacial water molecules were located with the program Water Analysis Package (22). Geometric parameters (S_c and the gap volume index) were calculated with Sc (15) and the protein-protein interaction server (23), respectively. Analysis of the interface was made using the PISA server (24). Interface residues were identified using CONTACT (15). Hydrogen bonds and salt bridges were identified using the programs WHAT IF and ESBRI (25, 26), respectively. Hydrophobic and non-canonical contacts were identified using the PIC server (27) with the following criteria: 5 Å for hydrophobic contacts, 4.5–7 Å for aromatic-aromatic interactions, and 6 Å for cation-π interactions. Electrostatic potentials were calculated with APBS (28). Figures were prepared using PyMOL (The PyMOL Molecular Graphics System, Version 1.2, Schrödinger, LLC) and ALINE (29).

RESULTS

General Features of the scFv 9004G-Cn2 Complex—Crystal structures of the scFv 9004G-Cn2 complex were determined in two different space groups. One structure, with three complexes in the asymmetric unit, was determined in the orthorhombic space group $P2_12_12_1$ at 2.5 Å resolution. A second structure, with two complexes in the asymmetric unit, was determined in the cubic space group F23 at 1.9 Å resolution (Table 1). Although the contacts of the two structures into the crystalline matrix are different (supplemental Fig. S1), the superposition of the scFv 9004G-Cn2 complexes gives a root mean square deviation value of ~0.6 Å (288 common residues). Each complex is composed of one Cn2 molecule and one scFv chain (V_H and V_L domains). The final model comprises residues 1–65 of Cn2 toxin, residues 1–117 of the heavy variable domain (V_H), and residues 132–239 of the light variable domain (V_L) of 9004G (residues of V_H and V_L are designated with superscripts ^{H} and ^{L}, respectively). The overall model geometry is good; residue $A183^L$ in the structure at 1.9 Å is the only amino acid located in a disallowed region of the Ramachandran plot (Table 1) due to its presence in a classic γ-turn of complementarity-determining region (CDR) L2 (30).

In the structure at 1.9 Å resolution, no electron density was observed for residue $R240^L$ of 9004G, the C terminus of Cn2 (Ser^{66}), and the residues in the interdomain linker between the

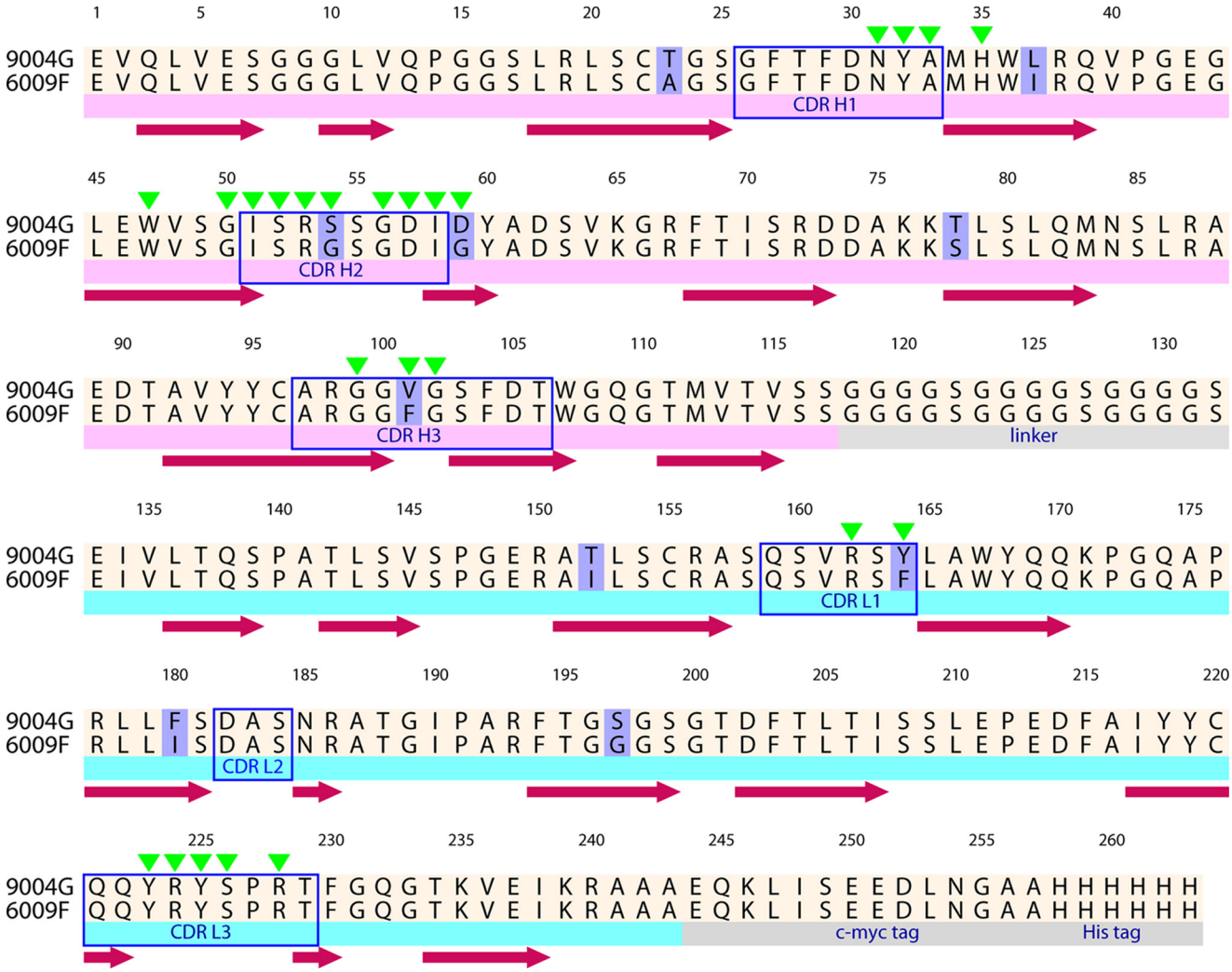

FIGURE 1. **Amino acid sequence of the neutralizing scFvs 9004G and 6009F.** The alignment of scFvs 9004G and 6009F with sequence changes is highlighted in *light purple*. Below the sequence of 6009F, the V_H (*light magenta stripe*) and V_L (*cyan stripe*) domains, as well as the 15-residue peptide $(Gly_4Ser)_4$ linker that connects V_H and V_L domains, and the c-Myc and His_6 tags (*gray stripes*) are marked. Secondary structure elements of 9004G are depicted with *brown arrows*. *Blue boxes* indicate the CDR regions of scFvs, whereas *green triangles* above the sequence of 9004G mark the residues that make direct or water-mediated interactions with Cn2 toxin in the reported scFv 9004G-Cn2 complex structure.

V_H and V_L domains (Fig. 1). In both structures, no electron density was visible for the C-terminal c-Myc and His_6 tags of scFv 9004G. Importantly, all regions not visible in the electron density maps are located far away from the complex interface (Fig. 2*a*) and are normally disordered in other scFvs crystal structures (31–34). The regions that comprise the interface of the complex are well defined, as indicated by the inspection of a simulated annealing difference omit map (Fig. 2*b*). Given the similarities between the two crystal structures, most of the analyses and conclusions presented herein will be those taken from the 9004G-Cn2 complex at the higher resolution.

The overall structure of the 9004G-Cn2 complex is shown in Fig. 2*a*. The complex involves five of the scFv CDR loops, which protrude into the concave surface of the Cn2 toxin. The V_H and V_L domains of the scFv 9004G exhibit the typical fold of the variable domains of an immunoglobulin, whereas Cn2 adopts the highly packed scaffold typical of scorpion β-toxins. The toxin α-helix (Asp^{23}–Tyr^{33}) is packed against a three-stranded antiparallel β-sheet, with four disulfide bridges stabilizing the core. These regular secondary structural elements are connected by irregular loops that cover much of the surface of the toxin. The β-turn (Asp^{7}–Thr^{10}) following the β_1 strand (Gly^{3}–Tyr^{4}) and the β-turn (Gly^{34}–Ala^{37}) running between the α-helix and the β_2 strand (Gly^{38}–Tyr^{42}) can be characterized as type I β-turns, whereas a type I′ β-turn (Tyr^{42}–Ala^{45}) connects β_2 and β_3 (Ala^{45}–Tyr^{51}) strands.

The Cn2 structure in the complex is similar to the structure determined by NMR (PDB code 1CN2 (35)). The superposition of the structure of Cn2 bound to scFv 9004G and the 15 reported NMR structural models gives an overall root mean square deviation value of 1.4 ± 0.1 Å (65 common residues). However, some differences exist between the crystal and the NMR structures (supplemental Figs. S2 and S3). In particular, the segment between residues Lys^{18} and Asp^{21} undergoes a significant rearrangement, which is probably due to the binding of the antibody (supplemental Figs. S2 and S3). In this region, the 15 reported NMR structural models compare much more closely with each other than they do with the crystal structure reported here. This rearrangement may result from steric hindrances between Lys^{18} and $D59^{H}$ and the repulsion between

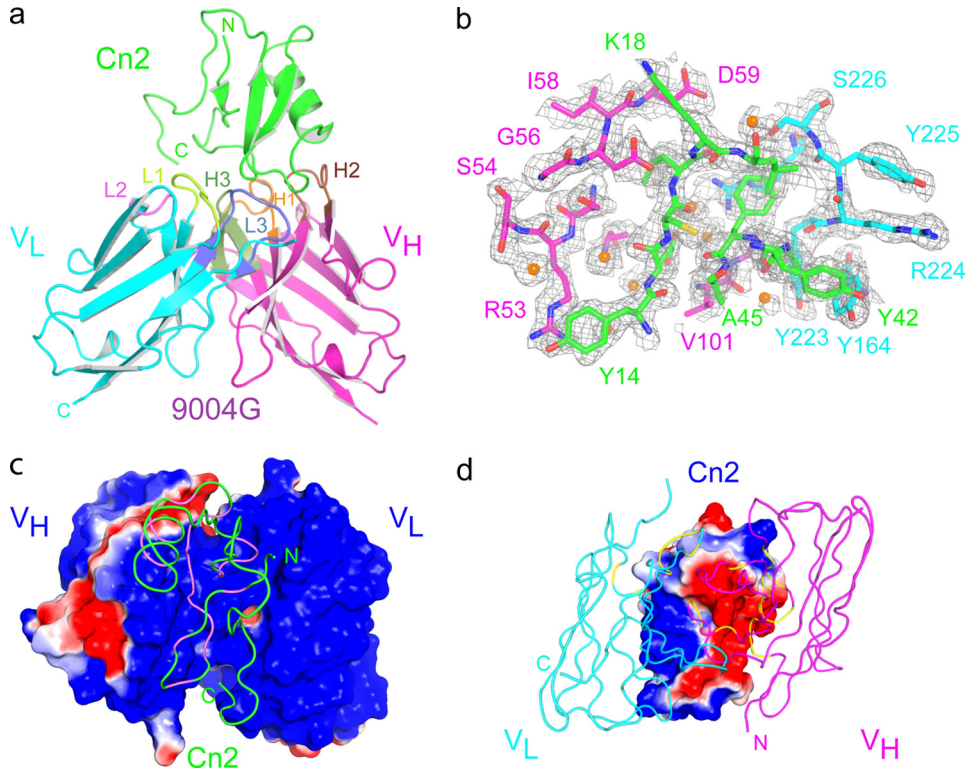

FIGURE 2. **Crystal structure of the complex between the scFv 9004G and the Cn2 toxin.** *a*, overview of the scFv 9004G-Cn2 complex at 1.9 Å resolution. The complex involves five of the scFv complementarity-determining region (CDR) loops, which interact with protruding loops of Cn2 toxin. Cn2 is colored in *green*. CDRs 1, 2, and 3 of the 9004G V_H domain (*magenta*) are colored *orange*, *brown*, and *green*, and CDRs 1, 2, and 3 of the V_L domain (*cyan*) are colored *lime*, *light magenta*, and *blue*. *b*, representation of several residues around the interface of the 9004G-Cn2 complex on a σA-weighted, $2F_o - F_c$ simulated annealing omit map, shown as a *gray mesh*. Residues are represented in *green* (Cn2), *magenta* (V_H domain), and *cyan* (V_L domain). The density for some water molecules (*orange spheres*) that mediate hydrogen bonds at the interface of the complex is located in the map. *c* and *d*, the chemical complementarity of the surfaces that build the interface of the complex contribute to the binding between 9004G and Cn2. The solvent-accessible surface of the proteins is colored according to its electrostatic potential. The antibody binding site is seen from the perspective of Cn2 (*c*) and from the perspective of 9004G (*d*). Note the highly negative (*red*) surface that protrudes from Cn2 (*d*) and interacts with the highly positive (*blue*) surface of the small grove at the center of the antigen binding site formed by the V_H and V_L domains of 9004G (*c*). Cn2 (*green*) and the V_H (*magenta*) and V_L (*cyan*) domains are drawn as *loops* and superposed on *c* and *d*, respectively. The segments of Cn2 that contact 9004G are colored in *violet*, and the segments of 9004G that contact Cn2 are colored in *yellow*.

opposite electrostatic surfaces between Asp^{21} and $D57^H$ after binding of 9004G (supplemental Figs. S2 and S3).

Shape and Chemical Complementarity between scFv 9004G and Cn2—Two parameters commonly used to characterize shape complementarity were calculated for the 9004G-Cn2 complex. One is the gap volume index, which evaluates how tightly the two subunits are packed by measuring the volume of empty space between them. The gap volume index for the 9004G-Cn2 complex is 2.4, indicating a shape complementarity similar to that found, for example, in enzyme-inhibitor complexes. This value is also within the average of 3.0 ± 0.8 reported for other antigen-antibody complexes (36, 37).

The second calculated parameter was the shape complementarity statistics score (S_c), a measure of the geometric fit at macromolecular interfaces. Its value for the scFv 9004-Cn2 complex is 0.78, which is higher than the average value (0.64–0.68) that has been reported for antibody-antigen complexes (37).

Moreover, the electrostatic potential, as seen in the solvent-accessible surface at the 9004G-Cn2 interface, is strikingly complementary (Fig. 2, *c* and *d*). On Cn2, the negatively charged epitope surface (Fig. 2*c*) complements with the positively charged paratope surface (Fig. 2*d*). Taken together, these parameters provide a quantitative characterization of the complex interface and indicate shape and electrostatic complementarity that are consistent with the known high affinity interaction observed between 9004G and Cn2 (12).

The scFv 9004-Cn2 Interface—Details of the scFv 9004G CDR contacts with Cn2 are presented in Figs. 1–3 and supplemental Table S1. The total buried surface area at the interface between scFv 9004G and Cn2 is ~1,700 $Å^2$. This value is similar to the average size for antigen-antibody complexes (38). The scFv 9004G contributes with 829 $Å^2$ of surface area (70% belongs to V_H domain; $V101^H$, $R53^H$, and $D57^H$ contribute with 37%), and Cn2 provides 873 $Å^2$ (Glu^{15}, Leu^{17}, and Phe^{44} contribute with 43%). Residue Leu^{17} contributes ~143 $Å^2$ to the buried surface area of Cn2, much more than any other residue in the complex (supplemental Table S3). As such, it qualifies as the "anchor" residue around which the remainder of the complex then adapts (39). At the center of the antigen binding site of 9004G, $V101^H$ protrudes from the cleft to interact with residue Glu^{15} in a small cavity surrounded by the hydrophobic cluster of Cn2 formed by Tyr^{42}–Ala^{45} (Fig. 3*c*). Residue $V101^H$ contributes to the total buried surface area with ~111 $Å^2$ and could be considered as an additional anchor residue (supplemental Table S3). At the periphery of the complex, $R53^H$ and $D57^H$ cooperate with 101 and 93 $Å^2$, respectively, and also act as molecular "latches" that lock the complex together (39).

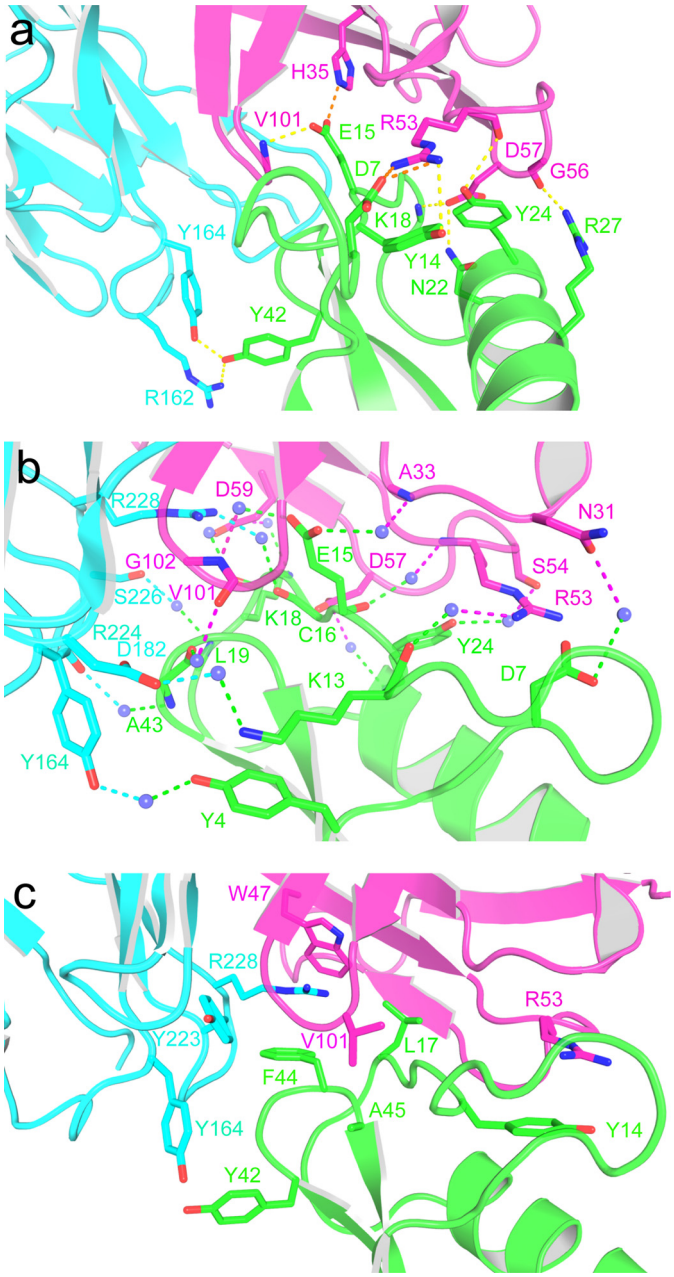

FIGURE 3. **The 9004G-Cn2 complex interface is mainly stabilized by charge-charge and hydrogen-bonding interactions involving five 9004G CDRs.** *a*, view of the charge-charge and hydrogen-bonding interactions between residues of the interface of the 9004G-Cn2 complex. Toxin Cn2 is colored in *green*, and V_H and V_L domains of 9004G are colored in *magenta* and *cyan*, respectively. The *yellow* and *orange dashes* represent hydrogen and charge-charge interactions, respectively. *b*, water-mediated hydrogen bonds at the 9004G-Cn2 interface. There are 15 water molecules (*blue spheres*) that interact with the same number of residues at the 9004G-Cn2 interface. The *magenta* and *cyan dashes* represent hydrogen bonds between residues of the V_H and V_L domains, respectively. Residue Glu^{15} is attached to the binding site of 9004G trough three water-mediated hydrogen bonds between 3 residues of 9004G. The other water-mediated hydrogen bonds are distributed along the interface. *c*, hydrophobic, aromatic-aromatic ($Y164^L$ with Tyr^{42}), and cation-π interactions ($R53^H$ with Tyr^{14} and $R228^L$ with Phe^{44}) at the 9004G-Cn2 interface. Note that these interactions are less represented than polar interactions and are located in the periphery of the interface of the complex. Interactions at the interface of the 9004G-Cn2 complex include 6 hydrogen bonds, 4 charge-charge interactions, 15 water-mediated contacts, and 45 van der Waals contacts. Details of these interactions are shown in Table 2 and supplemental Tables S1 and S2.

TABLE 2
Polar interactions between residues at the scFv 9004G-Cn2 interface

9004G location	9004G residue (atom)	Cn2 residue (atom)	Distance
			Å
Hydrogen bonds[a]			
CDR H2	$R53^H$ (NH_2)	Tyr^{14} (OH)	3.4
	$R53^H$ (O)	Tyr^{24} (OH)	3.4
	$G56^H$ (O)	Arg^{27} (NH_2)	3.0
	$D57^H$ (OD2)	Lys^{18} (N)	3.0
	$D57^H$ (OD2)	Asn^{22} (ND2)	2.9
CDR H3	$V101^H$ (N)	Glu^{15} (OE2)	2.9
CDR L1	$R162^L$ (NH1)	Tyr^{42} (OH)	3.0
	$Y164^L$ (OH)	Tyr^{42} (OH)	2.6
Salt bridges[a]			
Framework H2	$H35^H$ (NH1)	Glu^{15} (OE1)	2.7
CDR H2	$R53^H$ (NH_2)	Asp^7 (OD1)	3.2
	$R53^H$ (NH1)	Asp^7 (OD1)	2.9

[a] Criteria based on donor-acceptor distances ≤ 3.5 Å.

Polar and Hydrophobic Interactions of the scFv 9004-Cn2 Interface—CDRs H2 and L3 make the majority of the antigenic contacts (Fig. 2*a*). Four residues of the framework regions H2 ($H35^H$, $W47^H$, and $G50^H$) and H3 ($D59^H$) also participate in the binding of Cn2 (Fig. 3, *a* and *c*). The epitope of Cn2 recognized by 9004G is distributed through the segment that runs from the β_1 strand to the α-helix (Tyr^4, Asp^7, Tyr^{14}–Leu^{19}, and Asn^{22}) and includes part of the α-helix (Tyr^{24} and Arg^{27}) and the β-turn (Tyr^{42}–Ala^{45}) that connects the β_2 and β_3 strands. Two segments of Cn2, Lys^{13}–Leu^{19} and Tyr^{42}–Ala^{45}, form most of the contacts with 9004G (Fig. 3, *a*–*c*). Residue Glu^{15}, in the middle of the segment that runs between the β_1 strand and the α-helix, protrudes from the core of Cn2 and inserts into a cleft in the scFv binding site. The side chain of Glu^{15} nestles into a small cleft formed by hydrophobic and basic residues contributed by CDRs H1, H3, and L3: $A33^H$, $G99^H$, $G100^H$, $V101^H$, $G102^H$, and $R228^L$. Glu^{15} also forms a salt bridge with residue $H35^H$, which forms the cleft base. The side chain of Leu^{17} also inserts into a small cavity formed by residues from CDR H2: $I51^H$, $D57^H$, and $D59^H$. $W47^H$ and $G50^H$ form the cleft base (supplemental Table S2). The segment Tyr^{42}–Ala^{45} is flanked by CDR L1 and L3. Tyr^{42} forms an aromatic-aromatic interaction with $Y164^L$, and Phe^{44} rests over $R228^L$, forming a cation-π interaction (Fig. 3*c*). This segment also makes several polar interactions with 9004G (Table 2 and supplemental Tables S1 and S2).

The antigen binding site of 9004G is composed of the small cleft and three hydrophilic patches that surround it. Two patches have a positive electrostatic potential in their solvent-accessible surface. One of them is composed of several residues of CDRs L1 and L3: $R162^L$, $Y164^L$, $Y223^L$, $R224^L$, $Y225^L$, and $S226^L$. These residues form polar and hydrophobic interactions with Leu^{19}, Tyr^{42}, and Phe^{44} of Cn2 (Fig. 3, *a* and *c*). Residue Tyr^{42} nestles its side chain into a shallow cavity on the surface of V_L and forms hydrogen bonds with $R162^L$ and $Y164^L$ in addition to an aromatic-aromatic interaction with $Y164^L$ (Fig. 3*a* and Table 2). The second positive patch is composed by residues of CDRs H1 and H2: $Y32^H$, $S52^H$, $R53^H$, and $G56^H$. $R53^H$ forms two salt bridges with Asp^7 and a cation-π interaction with Tyr^{14} (Fig. 3*a* and Table 2). The main chain of $G56^H$ forms a hydrogen bond with Arg^{27}. This patch also makes several van der Waals interactions that involve Tyr^{14} and Tyr^{24} (supplemental Table S2). A patch with a negative electrostatic poten-

tial is located at the periphery of the binding site. This is composed by residues of CDR H2: $D57^H$, $I58^H$, and $D59^H$ that interact with a positive solvent-accessible surface patch of Cn2 formed by residues Leu^{17}, Lys^{18}, and Asn^{22} (Fig. 3). $D57^H$ forms two hydrogen bonds with Lys^{18} and Asn^{22}, as well as van der Waals interactions with Lys^{18} and Tyr^{24} (Fig. 3*a* and Table 2).

Water-mediated Hydrogen Bonds of the scFv 9004-Cn2 Interface—There are 15 invariant water molecules involved in water-mediated contacts at the interface of the 9004G-Cn2 complex. Invariant water molecules are defined as those that were observed among both complexes in the asymmetric unit of the structure at 1.9 Å resolution and interact with scFv 9004G and Cn2. Most of these are shown in Fig. 3*b* (see also supplemental Fig. S4). There are 15 hydrogen bonds between invariant water molecules and 9004G (10 with residues of V_H domain and 5 with residues of V_L domain) and the same number of additional bonds between the invariant water molecules and Cn2 (Fig. 3*b* and supplemental Table S1). These water molecules fill voids between the two proteins, although only a few of them contribute substantially to stabilize the antibody-toxin interface through enhancing the number of hydrogen bonds that knit the two proteins together. The invariant water molecules at the interface of the complex 9004G-Cn2 can be divided in two groups based on their locations and its *B*-values (supplemental Fig. S2 and supplemental Table S1). The five more ordered water molecules (those with lower *B*-values) are partially buried in a cavity at the center of the interface of the complex and are likely the most important for the stabilization of the complex (supplemental Fig. S2).

DISCUSSION

A combination of parameters that describe protein-protein interfaces shows that the interface of the scFv 9004G-Cn2 complex has a significant level of shape and chemical complementarity. The analysis of the interface of the complex identified residues in both proteins that dominate the formation and stabilization of the complex. The segments that run from the β_1 strand to the α-helix (Tyr^{14}–Leu^{19}) and the β-turn (Tyr^{42}–Ala^{45}) that connects the β_2 and β_3 strands interact with five of the 9004G CDRs (Fig. 2*a*). The most important Cn2 anchor residue is Leu^{17}, which inserts into a small cavity formed by residues of the V_H domain of 9004G. As in most of the protein-antibody interfaces (38), the analysis of the interface of the 9004G-Cn2 complex revealed that its stability is provided by van der Waals interactions, hydrogen bonds and, to a lesser extent, salt bridges. The salt bridges at the binding site probably are involved in the initial protein-protein association trough long range electrostatic interactions, whereas hydrogen bonds are the dominant force for the docking of the final complex (40).

Structural Basis of Scorpion Toxin Neutralization—Many of the biochemical details describing the residues of scorpion β-toxin Css4 from *C. suffusus suffusus* involved in its interaction with receptor site 4 of mammalian voltage-gated Na^+ channels have been recently uncovered (41). Indeed, a model depicting how Css4 might interact with the voltage sensor of Nav1.2 has been proposed (Fig. 4*a* and supplemental Fig. S5), (42). Cohen *et al.* (41) also suggested residues Glu^{28} and Gln^{32} as "hot spots" in the surface of interaction of Css4 with rat brain Na^+ channels. Residue Glu^{15} is conserved in mammalian scorpion β-toxins of the genus *Centruroides* (Fig. 4*a*) and plays a subtle role in the interception of the voltage sensor, according to the mechanism of the "voltage sensor-trapping" model of the voltage-gated sodium channels (43). When Glu^{15} is mutated to Arg on the recombinant toxins Css2 and Css4, the left shift of the voltage-dependent current assayed at rat brain channel $Na_v1.2a$ and rat brain channel $Na_v1.6$ is abolished (41, 44). In Cn2, residue Glu^{15} protrudes from the core of the toxin and is sequestered within a cavity at the center of the antigen binding site of 9004G (Fig. 4*c*).

Comparison of the functional surface of Css4 and the interface of the 9004G-Cn2 complex provides important clues for the molecular basis of the antibody-mediated toxin neutralization. Cohen *et al.* (41, 45) have shown that single substitutions in Phe^{14}, Phe^{17}, Leu^{19}, Asn^{22}, Tyr^{24}, Arg^{27}, Glu^{28}, Asn^{32}, Tyr^{42}, Phe^{44}, and Trp^{58} with alanine considerably decrease Css4 binding affinity to rat brain synaptosomes. In close correlation to these findings, here it is clearly demonstrated that residues Tyr^{14}, Leu^{17}, Leu^{19}, Asn^{22}, Tyr^{24}, Arg^{27}, Glu^{28}, Tyr^{42}, and Phe^{44} from Cn2 form part of the epitope recognized by 9004G (Fig. 4*a*). Because Css2, Css4, and Cn2 recognize $Na_v1.6$ channels (6, 8), it is highly likely that these toxins interact with a similar region of Na^+ channels and that Css2, Css4, and Cn2 share a similar region for the binding to $Na_v1.6$ channels (see supplemental Fig. S5).

The equivalent positions of Css4 that interact with rat brain Na^+ channels (41) are shown on Fig. 4*b* mapped on Cn2, whereas the epitope of Cn2 that is recognized by 9004G is shown on Fig. 4*c*. The epitope is located in one major segment around the α-helix and the region that connects the β_2 with β_3 of Cn2 and overlaps with the toxin region involved in the interaction of Na^+ channel, although this latter seems to cover a slightly larger area. Thus, the binding of 9004G to Cn2 precludes the interaction of a substantial part of the functional surface of Cn2 with Na^+ channels (43). In terms of structure-function relationships, we propose that this competition results in the potent neutralization effect of toxin Cn2 by the antibody scFv 9004G.

Structural Basis of Cross-reactivity of scFv 9004G—As scFv 9004G proved to neutralize both toxins, Cn2 and Css2, we mapped the sequence differences between them into the crystal structure of the complex 9004G-Cn2 (supplemental Fig. S6). Only residue 7 belongs to the interface region. The side chain of Asp^7 makes a salt bridge with the side chain of $R53^H$ in the scFv9004G-Cn2 complex (supplemental Fig. S6*a*). As this residue is substituted by serine in Css2, this interaction is probably lost in the putative complex (supplemental Fig. S6*b*). The loss of this interaction is probably reflected in the slightly different K_D values of 9004G for Cn2 and Css2, which are 0.21 and 0.81 nM, respectively (12).

Structure-Function Insight into the Evolution of the Different scFvs—We have analyzed a key change that took place during the maturation process of scFv 9004G. Mutation G59D (supplemental Fig. S8, *c* and *d*) increases recognition to Css2 in a significant manner (12). Both an increase in electrostatic interactions, in particular with residue Lys^{18} from the toxins, and an increased interaction surface with the toxin can be attributed to this higher affinity.

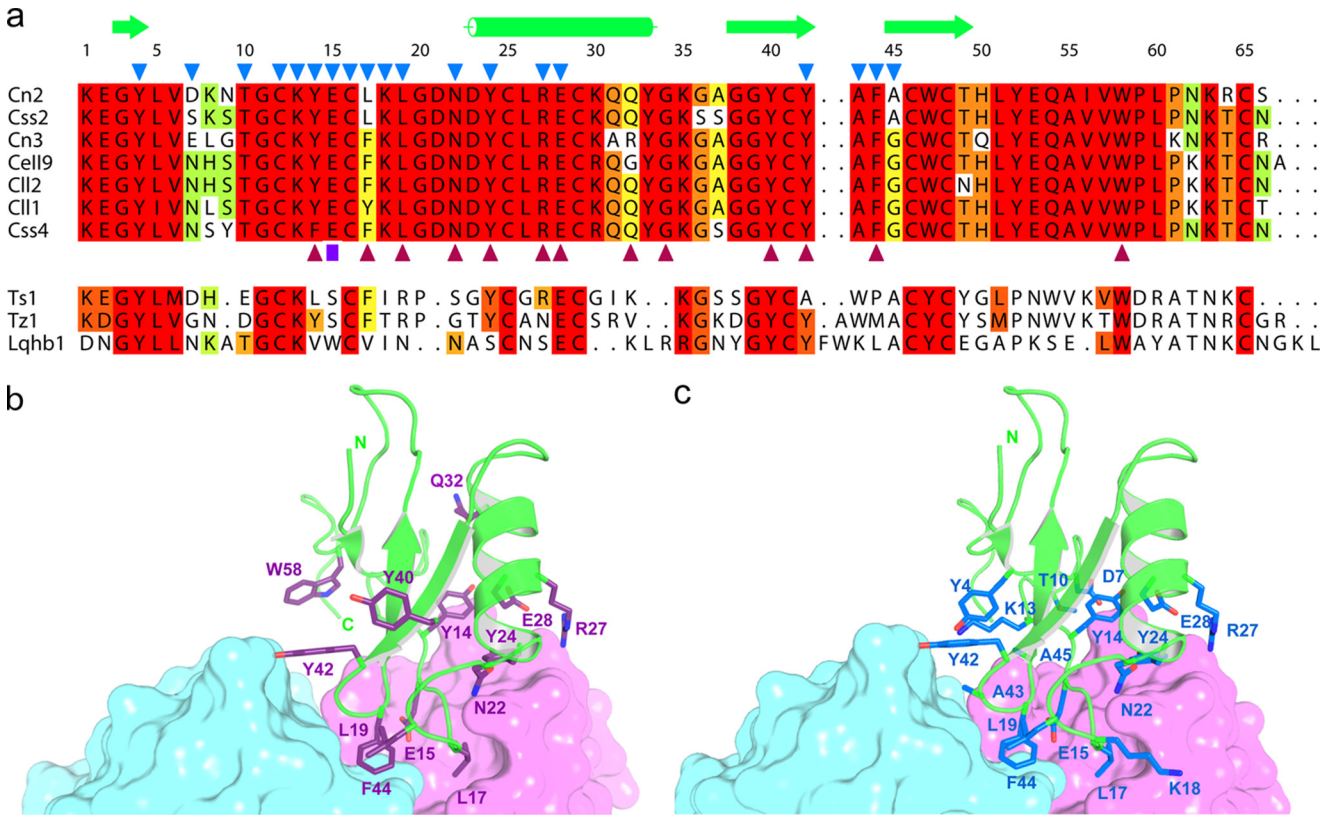

FIGURE 4. **The binding site of the Cn2 toxin to the scFv 9004G overlaps with its binding site to the mammalian Na^+ channels.** *a*, sequence alignment of representative scorpion β-toxins. The top group shows amino acid sequences of specific mammalian Na^+ channels β-toxins of the genus *Centruroides*. Amino acid residues highly conserved are highlighted in *red*. *Dots* indicate gaps inserted to maximize alignment. Numbering and secondary structure motifs in Cn2 (from this work) are indicated along the *top* of the alignment. *Blue triangles* in Cn2 mark residues that form the interface of the 9004G-Cn2 complex. *Purple triangles* below Css4 mark residues that are most important for the binding of Css4 to rat brain synaptosomes (41, 45). Abbreviations correspond to specific scorpion species: *Cn*, *C. noxius*; *Css*, *C. suffusus suffusus*; *Cll*, *Centruroides limpidus limpidus*; *Cell*, *Centruroides elegans*. The lower group shows sequences from β-toxins active on insects and mammalian Na^+ channels. Abbreviations correspond to scorpions: *Ts*, *Tityus serrulatus*; *Tz*, *Tityus zulianus*; *Lqh*, *Leiurus quinquestriatus hebraeus*. This group of toxins shares few of the residues that are important for the interaction of specific mammalian β-toxins with their receptors. Toxin sequences were compiled by Refs. 1, 49 and 50. *b*, toxin Cn2 is shown as a graphic representation and colored in *green*, whereas scFv 9004G is shown as surface presentation, with the V_H and V_L domains colored in *magenta* and *cyan*, respectively. Residues of Cn2 equivalent to residues important for the binding of Css4 to rat brain synaptosomes are colored in *purple*. *c*, the 9004G-Cn2 complex represented as in *b*. Residues of Cn2 that interact with 9004G are colored in *blue*. Residues Cys^{12} and Cys^{16} are not shown for clarity. A common binding region, comprising the segments that run from the β_1 strand to the α-helix (Tyr^{14}–Leu^{19}) and the β-turn (Tyr^{42}–Ala^{45}) that connects the β_2 and β_3 strands, is shared by the antibody 9004G and the Na^+ channels. These observations imply that 9004G neutralizes Cn2 by competing for a set of residues that form the bioactive surface of Cn2 and therefore blocks the receptor binding site.

We also modeled mutation $V101F^H$ (supplemental Figs. S6 and S7). This change on scFv 9004G, proposed from the sequence context and properties of scFv 6009F, yields scFv LR (12). This antibody has the highest protein yield of all scFvs previously tested, is more stable when compared with scFvs 6009F and 9004G, rescues mice from severe envenomation, and presents an increased affinity toward Css2 and Cn2. We detected two factors that could contribute to these properties. First, $F101^H$ could form a small, hydrophobic cluster with residues $Y164^L$ and $Y223^L$ (supplemental Fig. S7). It has been previously shown that the presence of this type of cluster can contribute to the stability of different proteins (46–48). Second, $F101^H$ could increase the number of atomic interactions with the toxin when compared with $V101^H$ in 9004G (supplemental Fig. S8, *a* and *b*), in particular by stacking interactions with Lys^{13} from the toxin. These examples show how the maturation process leads to progressively better antibodies with increased recognition and/or stability.

In summary, the 9004G-Cn2 interface has two principal features: complementarity between the interacting residues and the anchoring of essential residues for the binding of β-toxins to its receptor sites (Na^+ channels) into the antibody combining site. This identification of the first epitope of Cn2, a scorpion β-toxin that affects mammalian voltage-gated sodium channels, will certainly allow for the design of better antibodies against the venom of *C. noxius* and other scorpion venoms.

Acknowledgments—Data were collected at the Life Sciences Collaborative Access Team (LS-CAT) 21-ID-F and G beamlines at the Advanced Photon Source, Argonne National Laboratory. Use of the Advanced Photon Source was supported by the United States Department of Energy, Office of Science, Office of Basic Energy Sciences, under Contract DE-AC02-06CH11357. Use of the LS-CAT Sector 21 was supported by the Michigan Economic Development Corp. and the Michigan Technology Tri-Corridor for the support of this research program (Grant 085P1000817). The critical reading of Jonathan Ipsaro is greatly acknowledged. We thank Fredy Coronas, Sonia P. Rojas-Trejo, and Leopoldo Guereca for valuable technical assistance. We also thank Mónica Domínguez-Laguna for providing us the model of the 6009F-Cn2 complex.

REFERENCES

1. Possani, L. D., Becerril, B., Delepierre, M., and Tytgat, J. (1999) *Eur. J. Biochem.* **264,** 287–300
2. Gordon, D., Savarin, P., Gurevitz, M., and Zinn-Justin, S. (1998) *J. Toxicol. Toxin Rev.* **17,** 131–159
3. Jover, E., Couraud, F., and Rochat, H. (1980) *Biochem. Biophys. Res. Commun.* **95,** 1607–1614
4. Rodríguez de la Vega, R. C., and Possani, L. D. (2005) *Toxicon* **46,** 831–844
5. Couraud, F., Jover, E., Dubois, J. M., and Rochat, H. (1982) *Toxicon* **20,** 9–16
6. Estrada, G., Garcia, B. I., Schiavon, E., Ortiz, E., Cestele, S., Wanke, E., Possani, L. D., and Corzo, G. (2007) *Biochim. Biophys. Acta* **1770,** 1161–1168
7. Zamudio, F., Saavedra, R., Martin, B. M., Gurrola-Briones, G., Hérion, P., and Possani, L. D. (1992) *Eur. J. Biochem.* **204,** 281–292
8. Schiavon, E., Sacco, T., Cassulini, R. R., Gurrola, G., Tempia, F., Possani, L. D., and Wanke, E. (2006) *J. Biol. Chem.* **281,** 20326–20337
9. Chippaux, J. P., and Goyffon, M. (2008) *Acta Trop.* **107,** 71–79
10. Espino-Solis, G. P., Riaño-Umbarila, L., Becerril, B., and Possani, L. D. (2009) *J. Proteomics* **72,** 183–199
11. Riaño-Umbarila, L., Juárez-González, V. R., Olamendi-Portugal, T., Ortíz-León, M., Possani, L. D., and Becerril, B. (2005) *FEBS J.* **272,** 2591–2601
12. Riaño-Umbarila, L., Contreras-Ferrat, G., Olamendi-Portugal, T., Morelos-Juárez, C., Corzo, G., Possani, L. D., and Becerril, B. (2011) *J. Biol. Chem.* **286,** 6143–6151
13. Leslie, A. G. (1992) *Joint CCP4 + ESF-EAMCB Newsletters on Protein Crystallography,* No. 26, Collaborative Computational Project No. 4, Oxon, UK
14. Kabsch, W. (2010) *Acta Crystallogr. D. Biol. Crystallogr.* **66,** 125–132
15. Collaborative Computational Project, Number 4 (1994) *Acta Crystallogr. D. Biol. Crystallogr.* **50,** 760–763
16. McCoy, A. J., Grosse-Kunstleve, R. W., Adams, P. D., Winn, M. D., Storoni, L. C., and Read, R. J. (2007) *J. Appl. Crystallogr.* **40,** 658–674
17. Adams, P. D., Afonine, P. V., Bunkóczi, G., Chen, V. B., Davis, I. W., Echols, N., Headd, J. J., Hung, L. W., Kapral, G. J., Grosse-Kunstleve, R. W., McCoy, A. J., Moriarty, N. W., Oeffner, R., Read, R. J., Richardson, D. C., Richardson, J. S., Terwilliger, T. C., and Zwart, P. H. (2010) *Acta Crystallogr. D. Biol. Crystallogr.* **66,** 213–221
18. Emsley, P., and Cowtan, K. (2004) *Acta Crystallogr. D. Biol. Crystallogr.* **60,** 2126–2132
19. Langer, G., Cohen, S. X., Lamzin, V. S., and Perrakis, A. (2008) *Nat. Protoc.* **3,** 1171–1179
20. Laskowski, R. A., MacArthur, M. W., Moss, D. S., and Thornton, J. M. (1993) *J. Appl. Crystallogr.* **26,** 283–291
21. Sumathi, K., Ananthalakshmi, P., Roshan, M. N., and Sekar, K. (2006) *Nucleic Acids Res.* **34,** W128–W132
22. Praveen, S., Ramesh, J., Sivasankari, P., Sowmiya, G., and Sekar, K. (2008) *J. Appl. Crystallogr.* **41,** 952–954
23. Reynolds, C., Damerell, D., and Jones, S. (2009) *Bioinformatics* **25,** 413–414
24. Krissinel, E., and Henrick, K. (2007) *J. Mol. Biol.* **372,** 774–797
25. Vriend, G. (1990) *J. Mol. Graph* **8,** 52–56
26. Costantini, S., Colonna, G., and Facchiano, A. M. (2008) *Bioinformation* **3,** 137–138
27. Tina, K. G., Bhadra, R., and Srinivasan, N. (2007) *Nucleic Acids Res.* **35,** W473–W476
28. Baker, N. A., Sept, D., Joseph, S., Holst, M. J., and McCammon, J. A. (2001) *Proc. Natl. Acad. Sci. U.S.A.* **98,** 10037–10041
29. Bond, C. S., and Schüttelkopf, A. W. (2009) *Acta Crystallogr. D. Biol. Crystallogr.* **65,** 510–512
30. Al-Lazikani, B., Lesk, A. M., and Chothia, C. (1997) *J. Mol. Biol.* **273,** 927–948
31. Kaufmann, M., Lindner, P., Honegger, A., Blank, K., Tschopp, M., Capitani, G., Plückthun, A., and Grütter, M. G. (2002) *J. Mol. Biol.* **318,** 135–147
32. Arnett, K. L., Harrison, S. C., and Wiley, D. C. (2004) *Proc. Natl. Acad. Sci. U.S.A.* **101,** 16268–16273
33. Hwang, W. C., Lin, Y., Santelli, E., Sui, J., Jaroszewski, L., Stec, B., Farzan, M., Marasco, W. A., and Liddington, R. C. (2006) *J. Biol. Chem.* **281,** 34610–34616
34. Leysath, C. E., Monzingo, A. F., Maynard, J. A., Barnett, J., Georgiou, G., Iverson, B. L., and Robertus, J. D. (2009) *J. Mol. Biol.* **387,** 680–693
35. Pintar, A., Possani, L. D., and Delepierre, M. (1999) *J. Mol. Biol.* **287,** 359–367
36. Jones, S., and Thornton, J. M. (1996) *Proc. Natl. Acad. Sci. U.S.A.* **93,** 13–20
37. Decanniere, K., Transue, T. R., Desmyter, A., Maes, D., Muyldermans, S., and Wyns, L. (2001) *J. Mol. Biol.* **313,** 473–478
38. Lo Conte, L., Chothia, C., and Janin, J. (1999) *J. Mol. Biol.* **285,** 2177–2198
39. Rajamani, D., Thiel, S., Vajda, S., and Camacho, C. J. (2004) *Proc. Natl. Acad. Sci. U.S.A.* **101,** 11287–11292
40. Getzoff, E. D., Tainer, J. A., Lerner, R. A., and Geysen, H. M. (1988) *Adv. Immunol.* **43,** 1–98
41. Cohen, L., Karbat, I., Gilles, N., Ilan, N., Benveniste, M., Gordon, D., and Gurevitz, M. (2005) *J. Biol. Chem.* **280,** 5045–5053
42. Cestèle, S., Yarov-Yarovoy, V., Qu, Y., Sampieri, F., Scheuer, T., and Catterall, W. A. (2006) *J. Biol. Chem.* **281,** 21332–21344
43. Cestèle, S., Qu, Y., Rogers, J. C., Rochat, H., Scheuer, T., and Catterall, W. A. (1998) *Neuron* **21,** 919–931
44. Hernández-Salgado, K., Estrada, G., Olvera, A., Coronas, F. I., Possani, L. D., and Corzo, G. (2009) *Immunol. Lett.* **125,** 93–99
45. Cohen, L., Ilan, N., Gur, M., Stühmer, W., Gordon, D., and Gurevitz, M. (2007) *J. Biol. Chem.* **282,** 29424–29430
46. Van den Burg, B., Dijkstra, B. W., Vriend, G., Van der Vinne, B., Venema, G., and Eijsink, V. G. (1994) *Eur. J. Biochem.* **220,** 981–985
47. Machius, M., Declerck, N., Huber, R., and Wiegand, G. (2003) *J. Biol. Chem.* **278,** 11546–11553
48. Yun, Y. S., Nam, G. H., Kim, Y. G., Oh, B. H., and Choi, K. Y. (2005) *FEBS J.* **272,** 1999–2011
49. Gordon, D., Ilan, N., Zilberberg, N., Gilles, N., Urbach, D., Cohen, L., Karbat, I., Froy, O., Gaathon, A., Kallen, R. G., Benveniste, M., and Gurevitz, M. (2003) *Eur. J. Biochem.* **270,** 2663–2670
50. Leipold, E., Hansel, A., Borges, A., and Heinemann, S. H. (2006) *Mol. Pharmacol.* **70,** 340–347